Relative Intensity Noise and Four Wave Mixing in Multimode Elliptical Oxide Aperture VCSELs

Relative Intensity Noise and Four Wave Mixing in Multimode Elliptical Oxide Aperture VCSELs

C. Rimoldi[1], M. Novarese[1], L. L. Columbo[1], A. Tibaldi[1,2], P. Debernardi[2], S. Romero García[3], C. Raabe[3], and M. Gioannini[1]

1. Dipartimento di Elettronica e Telecomunicazioni, Politecnico di Torino, Corso Duca degli Abruzzi 24, IT-10129, Torino, Italy
2. Consiglio Nazionale delle Ricerca (CNR-IEIIT), Corso Duca degli Abruzzi 24, IT-10129, Torino, Italy
2. Cisco Optical, Nordostpark 12, D-90411, Nuremberg, Germany
cristina.rimoldi@polito.it

***Abstract*—We experimentally and theoretically characterize multimode elliptical VCSELs. Relative Intensity Noise spectra reveal spurious peaks and optical spectra show four-wave-mixing sidebands limiting the performance. We explain, for the first time, these nontrivial characteristics, drawing guidelines for designing VCSELs with low RIN over the modulation bandwidth.**

Keywords—VCSELs, elliptical aperture, relative intensity noise, multimode dynamics, mode coupling, frequency mixing.

I. Introduction

The attractive tradeoff between power and achievable bandwidth in multimode VCSELs has often identified them as good candidates for short-reach data transmission fiber links in datacenters [1]. Here, circular oxide aperture multimode VCSELs present the drawback of emitting several transverse modes distanced by only a few GHz, which is known to lead to performance issues, due to the beating among some of these modes, mediated by spatial hole burning, resulting in peaks in the relative intensity noise (RIN). Adopting elliptical oxide aperture VCSELs [2] is seen as a possible solution to this problem, since it leads to higher mode frequency separations to a point where any potential modal beating is beyond present-day receiver bandwidths. While this is a good short-term solution, when the requirement for higher speeds arises, the problem of peaks in the RIN is bound to re-emerge. Therefore, it is imperative to understand in depth the origin of such peaks, in order to find effective solutions to avoid them and improve the laser high-speed transmission performance. In this contribution, we characterize an 850 nm multimode VCSEL with an elliptical oxide aperture, measuring its near field and analyzing its optical and RIN spectra. The VCSEL has been designed to effectively suppress one polarization, in order to avoid any polarization switching effect. Our model, based on time-domain mode expansion and accounting for coherent mode coupling [3], can simulate the laser behavior in terms of modal PI, RIN spectrum, and optical spectrum and it can analytically explain the peaks present in the RIN spectrum as a result of four-wave mixing (FWM) process among transverse modes.

II. Experiment

In Fig. 1(a), we display the result of a near-field measurement of the VCSEL. The measurement was performed by collecting light at the output of the VCSEL through a 20x aspheric objective lens in order to obtain a far-field collimated beam. The laser beam is then passed through a series of 4 consecutive 750 nm blaze wavelength reflective diffraction gratings, the role of which is spatially separating transverse modes at different wavelengths. Finally, the gratings output is sent through a tube lens to a polarization-resolved compact camera. As a result of the measurement, in Fig. 1(a), we can observe five Hermite-Gauss transverse modes C_m. In Fig. 1(b), in orange, we report the laser experimental optical spectrum at I_{bias}=4.5 mA, collected through a high-resolution optical spectrum analyzer (Yokogawa, AQ6370D), where we can clearly identify the five lasing modes with the five main peaks at the frequencies $\nu_{1\text{-}5} \approx 0$, 194, 263, 413, 475 GHz, with the frequency of C_1 as reference frequency. Finally, in Fig. 1(c), in orange, we show its corresponding RIN spectrum, acquired with a 40 GHz RIN measurement system (SYCATUS, A0010-040).

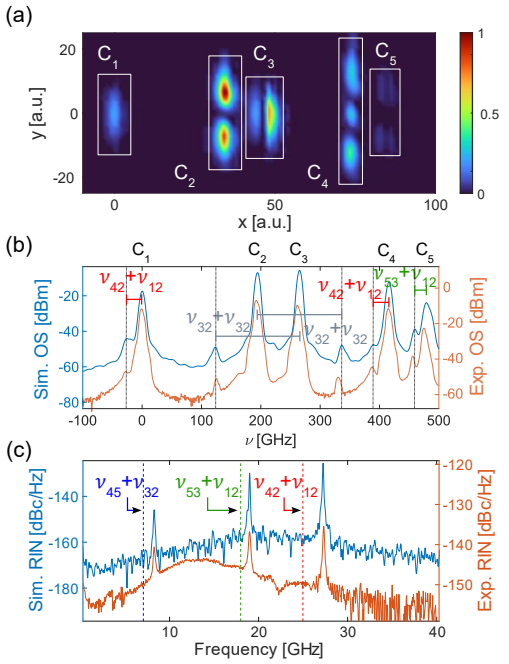

Fig. 1. (a) Near-field measurement of an 850 nm multimode VCSEL with an elliptical oxide aperture. C_m identifies the Hermite-Gaussian modes, of which we see the spatial intensity profile. (b) Experimental (in orange) and simulated (in blue) optical spectrum with labeled emitting modes. (c) Experimental (in orange) and simulated (in blue) RIN. The vertical dashed lines in (c) identify the predicted beating frequencies. The bias current is I_{bias}=4.5 mA. Other labels are illustrated in the text.

This work was partially supported by the European Union under the Italian National Recovery and Resilience Plan (PNRR) of NextGenerationEU, partnership on "Telecommunications of the Future" (PE00000001 - program "RESTART"). CR acknowledges funding from research contract no. [32-I-13427-1] (DM 1062/2021) funded within the Programma Operativo Nazionale (PON) Ricerca e Innovazione of the Italian Ministry of University and Research.

Here, we can clearly observe the presence of three peaks, at the frequencies of 8.3, 18, and 27.3 GHz.

III. Modeling and Results

Our model adopts a time-domain mode expansion approach, based on [4], modified to include the contribution of carrier diffusion in the transverse plane and spatial hole burning. The set of equations reads as follows:

$$\frac{d\tilde{E}_m(t)}{dt} = -\frac{1+i\alpha}{2\tau_{p,m}}\tilde{E}_m(t) + \\ +\frac{\Gamma G_N}{2}(1+i\alpha)\, e^{-i\omega_m t}\int_0^\infty\int_0^{2\pi}\rho d\rho d\varphi\,\frac{E}{1+\varepsilon N_p}C_m^*(N-N_0) + \\ +S_{sp}(t)e^{-i\omega_m t} \quad (1)$$

$$\frac{dN}{dt} = \frac{\eta_i I}{eV} - \frac{N}{\tau_e} - \frac{n_g^2\epsilon_0 G_N}{2\hbar\omega_0}\frac{|E|^2}{1+\varepsilon N_p}(N-N_0) + D\nabla_\perp^2 N, \quad (2)$$

where N, I, E, N_p are intended as functions of (ρ,φ,t), N being the carrier density, I the current, E the (slowly varying) electric field, and N_p the photon density. $\tilde{E}_m(t)$ relates to the projection of the electric field $E(\rho,\varphi,t)$ onto mode $C_m(\rho,\varphi)$

$$\tilde{E}_m(t) = e^{i\omega_m t}\int_0^\infty\int_0^{2\pi}\rho d\rho d\varphi\, E(\rho,\phi,t)\, C_m^*(\rho,\phi) \quad (3)$$

The linewidth enhancement factor is α, $G_N=g_N v$ with g_N the differential gain and v the group velocity, ε is the gain compression factor, and $S_{sp}(t)$ is the spontaneous emission. In the carrier density equation, η_i is the current injection efficiency, τ_e is the carrier lifetime, V is the volume of the active region, n_g is the group refractive index, and ϵ_0 is the vacuum permittivity. Finally, D is the carrier diffusion coefficient, $\nabla_\perp^2$ is the transverse Laplacian operator. Differently from other models present in literature, see for example [5], our approach properly accounts for frequency mixing and coherent transverse mode coupling, which allows for a correct description of the laser dynamics. Input experimental parameters in our simulator are the number of transverse modes relevant for the laser dynamics, the angular frequency detuning of each mode $\omega_m=2\pi\nu_m$ with respect to C_1, with angular frequency ω_0, as well as the modal photon lifetime $\tau_{p,m}$, which are tuned to match the threshold currents of the modes. As a result of a simulation at I_{bias}=4.5 mA, we obtain the optical spectrum displayed (in blue) in Fig. 1(b), where we can clearly identify the five lasing modes $C_{1\text{-}5}$. Further, in Fig. 1(c), we show (in blue) the simulated RIN spectrum, where we can clearly observe the presence of the same three peaks seen in the experiment, which demonstrates that our model is able to qualitatively simulate the laser RIN performance. The peaks in the spectral RIN can be analytically explained as follows. In the hypothesis that carriers are fast enough to follow the electric field, Eq. (2) can be solved in the adiabatic approximation. Under a few realistic approximations (including $|E|^2 \ll \frac{2\hbar\omega_0}{n_g^2\epsilon_0 G_N\tau_e}$), Eq. (1) can be reduced to

$$\frac{d\tilde{E}_m}{dt} = -\frac{1+i\alpha}{2\tau_{p,m}}\tilde{E}_m + \tilde{g}\Lambda\left(1-\gamma_{mmmm}\frac{|\tilde{E}_m|^2}{E_s^2} - \right. \\ \left. 2\sum_{n\neq m}\gamma_{mmnn}\frac{|\tilde{E}_n|^2}{E_s^2}\right)\tilde{E}_m - \tilde{g}\Lambda\sum_{n,l,r*}\gamma_{mnlr}\frac{\tilde{E}_n\tilde{E}_l\tilde{E}_r^*}{E_s^2}e^{i(\omega_{nm}+\omega_{lr})t} \quad (4)$$

With $\tilde{g} = \Gamma G_N(1+i\alpha)/2$, $E_s^2 = 2\hbar\omega_0/n_g^2\epsilon_0 G_N\tau_e$, $\Lambda = \tau_e(\eta_i I/eV - N_0/\tau_e)$, and, most importantly,

$$\gamma_{mnlr} = \int_0^\infty\int_0^{2\pi}\rho d\rho d\varphi\;\; C_m^*\, C_n C_l\, C_r^* \quad (5)$$

In Eq. (4) the first term on the RHS accounts for cavity loss and the contribution of the α factor, while the second term accounts for stimulated emission. The third and fourth terms are the self-saturation and the cross-saturation induced on the m-th mode by the emergence of the n-th mode, respectively. Finally, the fifth term accounts for the four-wave mixing process causing oscillation of $\tilde{E}_m$ at frequency $\omega_{nm}+\omega_{lr} = \omega_n - \omega_m + \omega_l - \omega_r$. Note that the sum on $n, l, r*$ is intended to already exclude the cases for which $n-m+l-r=0$. We highlight that the coefficients γ_{mnlr} can be null in some cases, depending on the spatial overlap of transverse modes. In the case of the considered elliptical VCSEL structure, the most relevant frequency beating conditions arising from the FWM term in Eq. (4) are the following:

$$\nu_{45}+\nu_{32} = \nu_4 - \nu_5 + \nu_3 - \nu_2 \approx 7 \text{ GHz} \quad (6)$$

$$\nu_{53}+\nu_{12} = \nu_5 - \nu_3 + \nu_1 - \nu_2 \approx 18 \text{ GHz} \quad (7)$$

$$\nu_{42}+\nu_{12} = \nu_4 - \nu_2 + \nu_1 - \nu_2 \approx 25 \text{ GHz} \quad (8)$$

The predicted frequencies are reported with vertical dashed lines in Fig. 1(c): here, we observe that Eq. (6-8) identify the peaks in the experimental (and simulated) RIN. We assume that the slight discrepancy between predicted and observed values is simply due to the approximations adopted to obtain an analytical form for Eq. (4). Focusing now on the optical spectra, the frequency separations in Eq. (6-8) should be observed as sidebands of the modes involved in each FWM process. While sidebands of the beating frequency in Eq. (6), as well as a few others, cannot be observed due to the limited OSA resolution bandwidth, a sideband associated to Eq. (7) can be observed around mode C_5 (in green), and sidebands associated to Eq. (8) are observed around mode C_1 and C_4 (in red). Additionally, we also observe two clear sidebands, highlighted in grey, which are also present in the experimental optical spectrum. These peaks are due to another FWM process with associated beating frequency $\nu_3 - \nu_2 + \nu_3 - \nu_2 \approx 138$ GHz, which cannot be observed through a RIN measurement due to the limited bandwidth of 40 GHz.

In conclusion, our experimentally validated model allows, through Eq. (6-8), to give a guideline for elliptical VCSEL design on the most relevant FWM processes that can affect noise performance and, consequently, the transmission performance, when VCSEL is employed for high-speed data transmission.

References

[1] V. Bhatt, et al., "Multimode Links Based on High-Speed VCSELs for Cost-Effective Data Center Connectivity", Optical Fiber Communication Conference (OFC) 2024, paper Th1B.4.

[2] D. Gazula, et al. II-VI Delaware Inc, "VCSEL with elliptical aperture having reduced RIN", US20190341743A1, 2020.

[3] C. Rimoldi, et al., "Dynamical analysis of multimode VCSELs with elliptical oxide aperture," Proc. SPIE 12904, Vertical-Cavity Surface-Emitting Lasers XXVIII, 129040L (2024).

[4] F. Prati, et al., "Pattern formation in lasers", Riv. Nuovo Cim., vol. 17, pp. 1-85 1994.

[5] A. Valle, et al., "Spatial holeburning effects on the dynamics of vertical cavity surface-emitting laser diodes", IEEE J. Quantum Electron., vol. 31, pp. 1423-1431, 1995.